Available online at www.sciencedirect.com

SciVerse ScienceDirect

Ceramics International 39 (2013) 903–909

CERAMICS INTERNATIONAL

www.elsevier.com/locate/ceramint

Review paper

Coating of nano-sized ionically conductive Sr and Ca doped $LaMnO_3$ films by sol–gel route

Hasan Okuyucu[a,*], Hanifi Cinici[b], Tulin Konak[b]

[a] Yıldırım Beyazıt University, Faculty of Engineering and Natural Sciences, Ulus, 06030 Ankara, Turkey
[b] Technical Education Faculty, Gazi University, Ankara 06500, Turkey

Received 16 February 2011; received in revised form 28 June 2012; accepted 4 July 2012
Available online 27 July 2012

Abstract

In this study, Sr and Ca doped $LaMnO_3$ thin ceramic films were coated on Al_2O_3 substrates by using a sol–gel route as the cathode material for SOFC. Nitrate precursors were used for the preparation of the thin film coating solution, and methanol and acetyl acetone were also used as the solvent and chelating agent, respectively. After the solution was prepared, an Al_2O_3 single crystal substrate was dipped into the solution. Then it was fired at 500 °C and annealed at 1025 °C for the crystallization. Coated films were characterized by X-ray diffraction (XRD), scanning electron microscopy (SEM), focused ion beam (FIB) and atomic force microscopy (AFM). Conductivity of the coated films was measured by the four probe Van der Pauw method. XRD, SEM, AFM and FIB characterizations of the coated film showed that the $LaMnO_3$ phase was formed, surface of the films was uniform and had homogenously distributed pores sized about 10 nm, mean grain size was about 60–80 nm and the film thickness was about 180 nm. The specific resistivity of the film was calculated to be 0.524 Ω m.

Keywords: A. Sol–gel; SOFC; $LaMnO_3$; Coating

Contents

1. Introduction

Solid oxide fuel cells (SOFCs) which operate with thin films have drawn great interest worldwide since they are productive and environmentally friendly [1,2]. SOFCs have advantages such as simplicity of their system and fuel variety. SOFCs have three main sections; cathode, anode and electrolyte. Since SOFCs are used at high temperature ($T > 800$ °C), anode, cathode and electrolyte materials should be stable at operation temperature [3–5]. Research has been increasing about improving the conductivity through the grain boundaries of nanocrystalline ceramics [3].

Cathode materials used in SOFCs should be stable in oxygen containing environment and should show good conductivity and enough catalytic activity under running conditions. For example, some complex oxides such as perovskites have very good electrical and ionic conductivities. $LaMnO_3$

*Corressponding author. Tel.: +90 312 324 15 55; fax: +90 312 32 41 505.
E-mail address: okuyucu@ybu.edu.tr (H. Okuyucu).

0272-8842/$ - see front matter © 2012 Elsevier Ltd and Techna Group S.r.l. All rights reserved.
http://dx.doi.org/10.1016/j.ceramint.2012.07.010

(LMO), which has a perovskite structure, is used as a cathode material in SOFCs. It is known that crystalline ceramics which have the $LaMn_xM_{(1-x)}O_3$ structure (M: transition metals; Fe, Co, Cr, Mn) show high ionic/electrical conductivity at temperatures above 800 °C. It is also known that Sr doped LMO is chemically stable on the cathode/electrolyte interface [6,7]. Lanthanum ferrite ($LaFeO_3$) and lanthanum cobaltite have been used as cathode materials for SOFCs [8,9]. $LaCoO_3$ has a higher ionic conductivity than $LaMnO_3$. However, thermal expansion coefficient of $LaCoO_3$ is higher than that of $LaMnO_3$ under same conditions. For this reason, $LaMnO_3$ is very suitable as a cathode material for SOFCs. $LaFeO_3$ has a good thermal expansion coefficient value. However, its conductivity is low [10,11]. It is also known that the mixed $La(Sr)Fe(Co)O_{3-1}$ (LSCF) ceramic material has optimum conductivity and thermal expansion coefficient value [12,13].

Perovskite structured LMO, SrO and CaO doped LMOs have been used as cathode materials [14]. Lanthanum manganate and other cathode materials for SOFCs have been coated as thin films by electroferritic coating [14], PVD [15], and spray pyrolysis [16]. The sol–gel method has been used to produce LMO powders [17] but never been used as a coating method.

Since ions in ionic conductive solids move from their own place to another similar place with thermal activation, in most ionic conductive solids, a high temperature is needed to show ionic conductivity. αAgI and some Ag and Li based oxides and sulfides are known as low temperature ionic conductors [3]. This property can be attributed to their high level of structural imperfections and open channels between ionic positions.

Grain boundaries in traditional conductive metallic materials show imperfections from the point of conduction. For this reason, conductivity of a metallic material decreases with decreasing grain size. However, it is known that grain boundaries in ionic conductive materials increase the conductivity [3,18,19]. In a crystalline ionic structure, the lesser the grain size the more the conductivity. It is reported in a previous study that conductivity in grain boundaries have more than in other areas [3]. It can be concluded that there are more vacancies in grain boundaries and the atoms in grain boundaries are bounded with weaker bonding.

In this study, coating and characterization of pure and Sr and Ca doped LMO thin films on Al_2O_3 single crystal were investigated. Films were characterized by means of XRD, SEM, AFM, and FIB. Ionic conductivity of the LMO thin films was measured with the four probe Van de Pauw method.

1.1. Experimental methods

In this study, different chemicals were coated on glass. A homogeneous coating was obtained from the solutions prepared by lanthanum (III) nitrate hexahydrate ($La(NO_3)_3 \cdot 6H_2O$) and manganese (II) nitrate hydrate ($Mn(NO_3)_2 \cdot xH_2O$). To prepare a stoichiometric coating, La/Mn molar ratio of nitrate precursors was kept at 1/1. Solutions were stirred for 24 h altogether with acetyl acetone ($C_5H_8O_2$) and methanol (CH_3OH) used as the chelating agent and solvent, respectively. Then, a completely transparent LMO solution was obtained with a soft-pink color.

Sr and Ca doped LMOs were coated on the substrates by the sol–gel process using the strontium nitrate ($Sr(NO_3)_2$) and calcium nitrate hexahydrate ($Ca(NO_3)_2 \cdot x4H_2O$), respectively. In addition to pure LMO, $La_{1-x}Ca_xMnO_3$ and $La_{1-x}Sr_xMnO_3$ thin films were coated on single crystal substrate.

For the coating process, solution was firstly coated on a glass sheet with dimensions $10 \times 10 \times 0.5\ mm^3$ to investigate the success of the coating process. After deciding the optimum coating solution, single crystalline Al_2O_3 pieces were coated with the same procedure. After the coating process of glass or single crystal Al_2O_3 pieces, a vertical furnace was used for burning and/ or drying purposes. A simple fixture was created in our laboratory to transfer the coated pieces from within the solution to the preheated furnace.

Although thermal expansion coefficients of the substrate Al_2O_3 and the coating LMO are very low, drying/burning temperature was chosen as 500 °C which was much lower than the crystallization temperature to eliminate the thermal shock problem. However, time for evaporation of the solution and sticking to the substrate surface is short enough at 500 °C. Moreover, the substrate was dipped into the solution more than once.

Crystallization heat treatment process was applied on the substrates which were coated with an amorphous layer. Crystallization annealing was applied to the coated substrates at 850 °C, 925 °C, 975 °C, and 1025 °C for 10 min.

The phases present in the coated films were determined by XRD using a Rigaku DMAX 2200 machine. XRD was performed on the samples with Cu-Kα radiation at 40 kV/40 mA with a scanning angle interval from 25° to 60° in 2θ with a scan speed of 2.0°/min. For the comparison of the positions of the diffracted planes obtained from the XRD results, Joint Committee on Powder Diffraction Standards (JCPDS) files were used.

Surface characterization of the films was determined with a FEI–SEM (Nova 600i Nanolab). Thickness of the films was determined with a focused ion beam (FIB) aparatus attached to the SEM. Surface profilometry of the films was determined with atomic force microscopy (XE–100E PSIA).

High temperature ionic conductivity of the films was measured by a four-point current/potential measurement Van der Pauw [20] fixture with a high temperature aparatus (Therm-A-STAT, ELIMKO). As seen in Fig. 1, voltage was given on the film with two electrodes and resistance was measured with other two electrodes attached to the film.

Specific resistivity of the films was determined using Eq. (1) from the four point Van der Pauw technique [20]. Electrodes were attached to the film surface from the points: A–D as seen in Fig. 1. Resistivity $R_{AB,CD}$ is the resistivity formed between point C and D as a result of the current between A and B. Resistivity $R_{BC,DA}$ was also measured with the same

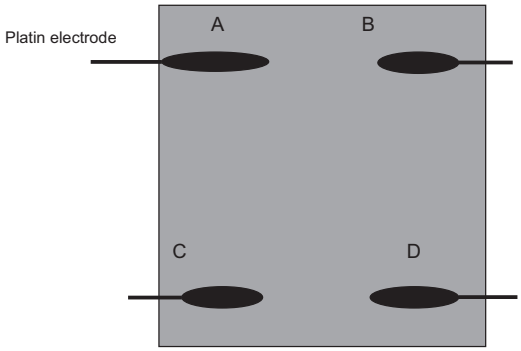

Fig. 1. Schematic representation of placing the electrodes on the thin film surface in theVan der Pauw method.

procedure. Specific resistivity was calculated as

$$\rho = \frac{\pi d}{ln\,2}\left[\frac{R_{AB,CD}+R_{BC,DA}}{2}\right] f\left(\frac{R_{AB,CD}}{R_{BC,DA}}\right)\ \Omega\ cm\ [20] \quad (1)$$

In this formula, "d" is the thickness. "f" is the correction factor when $R_{AB,CD}$ and $R_{BC;DA}$ resistivities were measured differently. This correction factor "f" was calculated from the equation

$$f\left[\frac{R_{AB,CD}}{R_{BC,DA}}\right] = 1-\left[\frac{R_{AB,CD}-R_{BC,DA}}{R_{AB,CD}+R_{BC,DA}}\right]\frac{\ln(2)}{2}-\left[\frac{R_{AB,CD}-R_{BC,DA}}{R_{AB,CD}+R_{BC,DA}}\right]^4 \times\left[\frac{(ln(2))^2}{4}\right]-\left[\frac{(ln(2))^3}{12}\right][20] \quad (2)$$

Correction factor was used when the film surface was not homogeneous. In this case, specific resistivity was calculated as

$$\rho = \left[\frac{\pi d}{ln\,2}\right] R_{AB,CD}[20] \quad (3)$$

When the film was coated on Al_2O_3 substrate, conductivity of the film was measured. However, surface characterization of the film and film thickness could not be measured because Al_2O_3 substrate was an insulator. For the surface characterization and film thickness measurements, films were coated on silicon substrates because silicon shows an interaction with the electrons created by SEM. Conductivity of the coated films was measured with the Van der Pauw method as seen in Fig. 1. The measurements were performed in air.

2. Resuls and discussion

XRD results of LMO thin films dipped twice into the solution and fired at 500 °C are presented in Fig. 2. In the sol–gel dip coating, films were not crystalline after the firing at 500 °C as seen from the XRD results of fired thin films in Fig. 2 because only the XRD peak of Al_2O_3 substrate was observed after the firing operation. Moreover, it is known that thin films must be crystalline to become conductive.

Coated films were first annealed at 850 °C; after this annealing operation, annealing temperature was increased

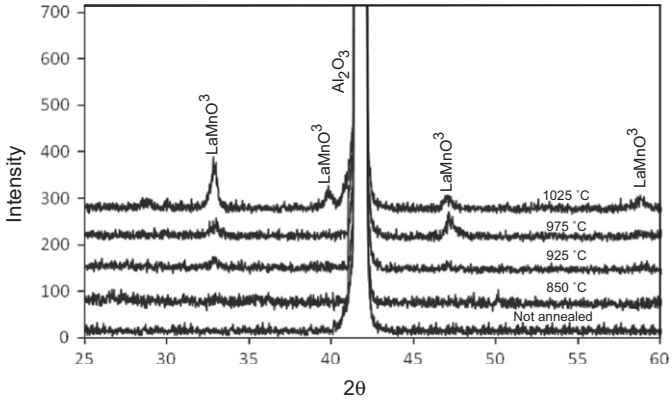

Fig. 2. XRD of LMO thin film coated on Al_2O_3 single crystal by two times dipped, fired at 500 °C and annealed at various temperatures.

to 925 °C, 975 °C, and 1025 °C gradually. Coated films that were dipped twice (films were fired at 500 °C after each dipping) were annealed at 850 °C, 925 °C, 975 °C and 1025 °C. It is known from the literature that LMO powders were calcined at temperatures between 700 °C and 1100 °C previously [21,22].

XRD results of LMO thin films that are two times dipped and then annealed at different temperatures are given in Fig. 2. The first LMO peak was seen after the annealing at 925 °C as seen in Fig. 2.

Perovskite structures could contain vacancies because the B atom at in the center of the cube may have different valence values. When the number of these vacancies is low, they disperse randomly. Manganese in the structure of LMO is a transition metal and having different valences such as Mn^{3+} and Mn^{4+} leads to vacancy formation. When the number of these vacancies is increased, they become ordered. Ionic conductivity increases with increasing vacancy concentration. Ionic conductivity of the LMO structure, vacancy concentration and conductivity are increased by doping the structure with La, Sr, and Ca ions [23].

Homogeneous thin films were obtained with the coating of LMO, $La_{1-x}Ca_xMnO_3$ or $La_{1-x}Sr_xMnO_3$ on the single crystal substrates. $La_{1-x}Ca_xMnO_3$ and $La_{1-x}Sr_xMnO_3$ phases and smooth surfaces were obtained in the coatings doped with Ca and Sr ions, respectively. XRD results of $La_{1-x}Ca_xMnO_3$ and $La_{1-x}Sr_xMnO_3$ coated thin films are presented in Fig. 3. As seen from the XRD patterns in Fig. 3, there is no secondary phase in the films. At 1025 °C, the $La_{1-x}(Sr,Ca)_xMnO_3$ peak was distinguished and certain boundaries of the peaks were seen clearly (Fig. 3).

As seen in Fig. 2, for $LaMnO_3$, which is annealed at 1025 °C, the orthorhombic structure has diffraction angles at 32.6°, 40.103°, 46.824° and 58.306° in 2θ which correspond to JCPDS #: 89-2470. Corresponding peak intensities were not very high because of the low film thickness.

LMO can be orthorhombic, rhombohedral or cubic depending on the Mn^{4+} concentration. When the Mn^{4+} concentration is about 0–12%, 18–30%, and more than 30%, LMO becomes orthorhombic, rhombohedral, and

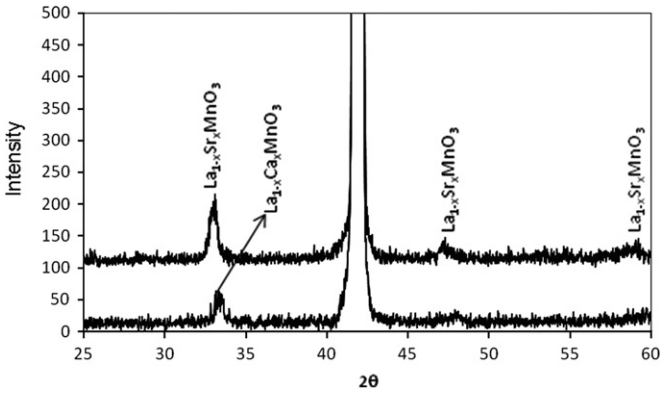

Fig. 3. XRD scanning of Sr and Ca doped LMO thin film coated on Al_2O_3 single crystal by two times dipping and firing at 500 °C and annealing at 1025 °C.

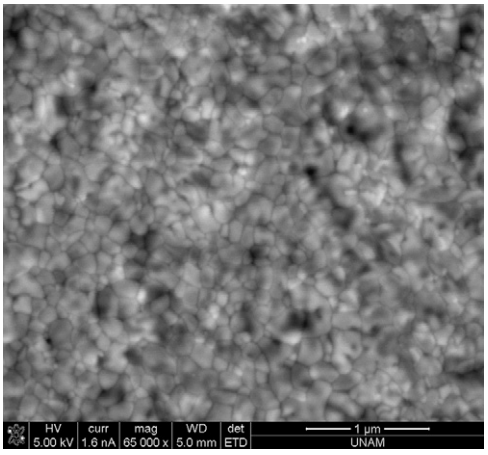

Fig. 4. SEM image of sol–gel coated LMO thin film annealed at 1025 °C.

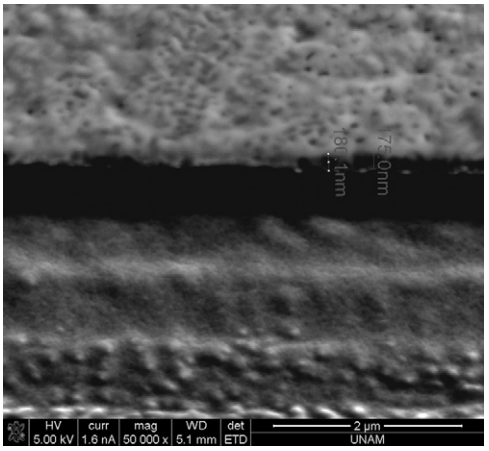

Fig. 5. SEM image of two times dipped LMO film ionically etched and bended with an angle of 53°.

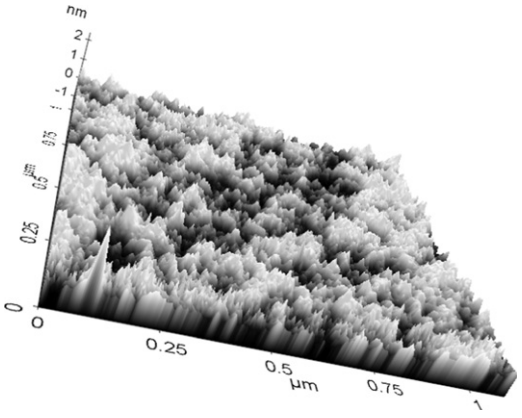

Fig. 6. AFM surface profilometry of LMO thin film coated on Al_2O_3 single crystal by using nitrate precursors before the annealing.

cubic, respectively. Above 800 °C, the cubic phase is observed in LMOs [24]. It can be said that Mn^{4+} concentration of the orthorhombic phase given in Fig. 2 is less than 12%.

As seen from the images taken with SEM, the coating surface has homogeneous appearances. From the images in Figs. 4 and 5, the thin film has a grainy structure and the mean grain size is about 60–70 nm. Grains were homogenously structured and the film has very low porosities with a size of 8–10 nm. These porosities diminish the conductivity values [25]. However, since the porosities are very few, conductivity of the film did not diminish dramatically. The thin film is grain size of 60–70 nm in this study is similar to the grain size of 57 nm coated with a chemical vapor deposition method [15]. However, the thickness 1 µm of the thin film coated with a chemical vapor deposition is much larger than the thin film thickness of 60 nm produced in this study.

The ionically etched region of the coated film was bent up to 53° and the images were taken from the thin film cross-section by SEM. As seen from the images, the thickness of the film dipped twice is about 180 nm. Substrates were dipped into the coating solution and then fired at 500 °C for 10 s. After firing the coated films, they were still amorphous. Since the coated film is crystallized after the annealing, diffusion takes place during this crystallization. A layered film was not observed although it was dipped twice.

As seen from Fig. 5, the film was coated to the substrate perfectly. There is no vacancy or an unsticking region between the thin film and the substrate. It can be said that the bond between film and substrate is strong.

It is known that the thickness of the film in sol–gel coating depends on gravity, viscosity of the solution, flowing angle of the solution on the substrate after taking out of the solution, value of bonding force between thin film and substrate, and differences of surface tension. The film thickness should be controlled by changing these parameters. However, the control of the firing rate was very difficult for the manually controlled dip coating systems.

In Fig. 6 AFM surface profilometry of coated film before the annealing is given. AFM mapping also proved that coated films were homogenous before and after the crystallization heat treatment. As seen in Fig. 6, the thin

film is fully coated on the single crystal substrate. Before the crystallization annealing, the surface of the coated film is like needle shaped with small grains of about 3–5 nm. This thin film was fully amorphous. After heat treating the thin film at 1025 °C, the structure was crystallized and grains are grown (Figs. 2 and 7). As seen from Fig. 5, the film has very less porosity and a homogenous distribution of grain size compared with some other coated ionic conductive films [26]. Mean grain size of the coated film is almost the same as that of the other coated film [26,27]. Needle shaped grain growth become much larger after heat treatment for crystallization. However, the surface was still homogenous after the crystallization while surface roughness increased after the crystallization.

Since the film has high resistance values at low temperatures, resistance measurement of the thin films was not performed below 550 °C. Resistance of the films was measured between 550 and 925 °C. The relation between resistance and temperature values of LMO films is presented in Table 1 and a graph of this relation is given in Fig. 8. Specific resistivity was calculated using the

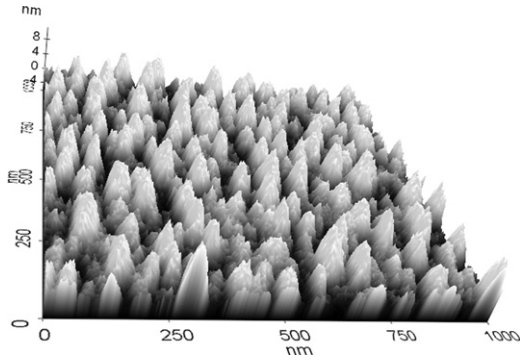

Fig. 7. AFM surface profilometry of LMO thin film coated on Al_2O_3 single crystal by two times dipping and firing at 500 °C and annealing at 1025 °C.

Table 1
Resistance values of the LMO thin film measured with the four point probe Van der Pauw method at various temperatures.

Temperature (°C)	$R_{AB,CD}$ (Ω m)
550	63,140
575	44,638
600	39,072
625	33,787
650	26,061
675	21,322
700	19,572
725	17,304
750	14,971
775	11,807
800	9813
825	8504
850	7868
875	7268
900	6901

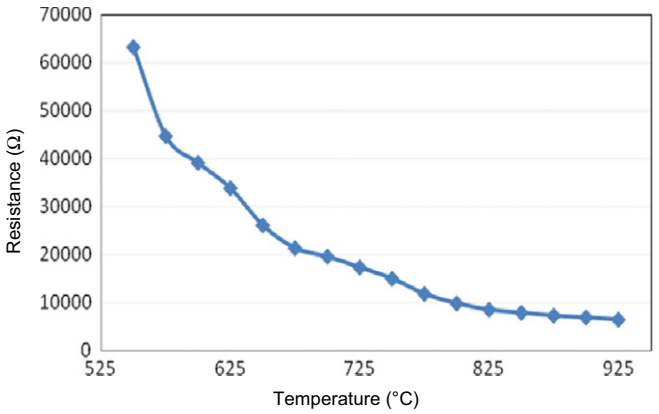

Fig. 8. Relationship between resistance and temperature of $LaMnO_3$ thin film coated on Al_2O_3 single crystal.

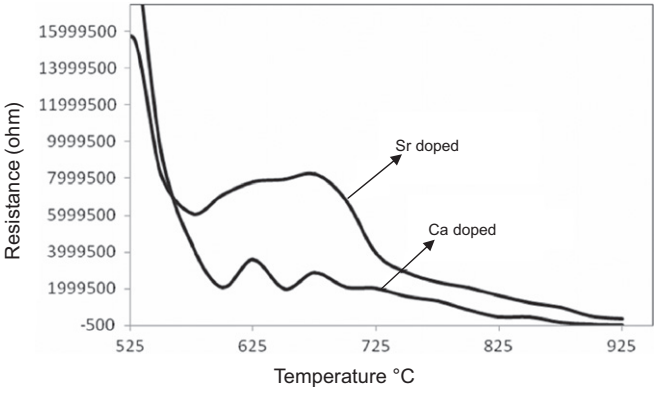

Fig. 9. Relationships between resistance and temperature of $La_{1-x}Ca_xMnO_3$ and $La_{1-x}Sr_xMnO_3$ thin films coated on Al_2O_3 single crystal.

experimental values with Eq. (3). Calculated specific resistivity of the coated LMO thin film is 0.524 Ω cm. The CVD coated $LaMnO_3$ film showed a conductivity of 4,8 S/cm at 560 °C [28]. This conductivity corresponds to a specific resistivity of 0.208 Ω cm which is slightly lower than the resistivity value found in this study.

For each of the three I-V measurements, the resistance of the coated films decreased with increasing temperature and the conductivity increased with increasing temperature. It can be said that thermal vibration increases with increasing temperature and ions reach an appropriate energy level to overcome the energy barrier. It is known that point defects like Schottky, Frenkel and atomic vacancies increase the ionic conductivity. Increasing the temperature increases the thermal activation and the number of point defects consequently increasing the ionic conductivity too.

Ionic conductivity of the perovskite structured oxides increases with doping of Sr and Ca ions [29]. However, Sr and Ca doped films showed higher resistance in this study as seen in Fig. 9.

Solution concentration and waiting time between the taking the coated substrates out of the solution and putting them into the furnace are the factors which affect

the film thickness of sol–gel coating. Even though these factors are controlled, it is very difficult to control the film thickness precisely. Sometimes a thick film could be obtained although a thin film is aimed. A variation in thickness can affect the resistivity, too.

The relationship between resistance and temperature of the thin films above 550 °C is given in Fig. 9. The resistance was very high at 550 °C while it lowered continuously above a temperature of 600 °C.

The relationship between resistance and temperature of $La_{1-x}Sr_xMnO_3$ thin film is given in Fig. 9. As seen in this figure, the resistance value decreased while conductivity increased with increasing temperature.

Resistance is continuously decreased over 675 °C. Four point measured resistance and resistivity of pure $LaMnO_3$ with a thickness of 180 nm was 6432 Ω and 0.524 Ω cm, respectively. Four point measured resistance and resistivity of Ca doped $La_{1-x}Ca_xMnO_3$ with a thickness of 180 nm was 40165 Ω and 3.275 Ω cm, respectively. Four point measured resistance and resistivity of Sr doped $La_{1-x}Sr_xMnO_3$ with a thickness of 180 nm was 346,769 Ω and 28.279 Ω cm, respectively.

3. Conclusion

In this study, $LaMnO_3$ ceramic thin films were coated on Al_2O_3 single crystals as cathodes for a possible solid oxide fuel cell. A sol–gel method is employed to coat this thin film and it can be said that it is very effective for coating such films. Conductivity of the coated films is in a reasonable range. It can be seen from the cross-section that there is no unsticking region between the thin film and substrate; the film is coated on the substrate perfectly. Mean grain size of thin film is about 60–70 nm and each dipping gives a 80–90 nm thickness. It can be concluded that this study showed that the sol–gel method can be employed preferably instead of CVD, PVD and plasma spray coating. Although several different coating applications have been applied with sol–gel based methods, our method gave a homogeneous contribution of grain size and film thickness.

Acknowledgments

The authors would like to thank the financial support rom the TUBITAK project (# 105M280).

References

[1] A. Boudghene Stambouli, E. Traversa, Solid oxide fuel cells (SOFCs)—a review of an environmentally clean and efficient source of energy, Renewable and Sustainable Energy Reviews 6 (2002) 433–455.

[2] I.V. Yentekakis, T. Papadam, G. Goula, Electricity production from wastewater treatment via a novel biogas-SOFC aided process, Solid State Ionics 179 (2008) 1521–1525.

[3] H.L. Tuller, Ionic conduction in nanocrystalline materials, Solid State Ionics 131 (2000) 143–157.

[4] T. Komatsu, R. Chiba, H. Arai, K. Sato, Chemical compatibility and electrochemical property of intermediate-temperature SOFC cathodes under Cr poisoning condition, Journal of Power Sources 176 (2008) 132–137.

[5] C. Monterrubio-Badillo, H. Ageorges, T. Chartier, J.F. Coudert, P. Fauchais, Preparation of $LaMnO_3$ perovskite thin films by suspension plasma spraying for SOFC cathodes, Surface and Coatings Technology 200 (2006) 3743–3756.

[6] S.P. Jiang, Issues on development of (La,Sr)MnO_3 cathode for solid oxide fuel cells, Journal of Power Sources 124 (2003) 390–402.

[7] C.H. Chen, H. Kruidhof, H.J.M. Bouwmeester, A.J. Burggraaf, Preparation of gas-tight strontium-doped lanthanum cobaltate by an aqueous sol–gel process, Materials Science and Engineering B 39 (1996) 129–132.

[8] S.J. Skinner, Recent advances in Perovskite-type materials for solid oxide fuel cell cathodes, International Journal of Inorganic Materials 3 (2001) 113–121.

[9] M. Gödickemeier, K. Sasaki, L.J. Gauckler, I. Riess, Perovskite cathodes for solid oxide fuel cells based on ceria electrolytes, Solid State Ionics 86–88 (1996) 691–701.

[10] G.Ch Kostogloudis, Ch Ftikos, Properties of A-site-deficient $La_{0.6}Sr_{0.4}Co_{0.2}Fe_{0.8}O_{3-\delta}$ based perovskite oxides, Solid State Ionics 126 (1999) 143–151.

[11] A. Petric, P. Huang, F. Tietz, Evaluation of La–Sr–Co–Fe–O perovskites for solid oxide fuel cells and gas separation membranes, Solid State Ionics 135 (2000) 719–725.

[12] M.T. Colomer, B.C.H. Steele, J.A. Kilner, Structural and electrochemical properties of the $Sr_{0.8}Ce_{0.1}Fe_{0.7}Co_{0.3}O_{3-\delta}$ perovskite as cathode material for ITSOFCs, Solid State Ionics 147 (2002) 41–48.

[13] L.-W. Tai, M.M. Nasrallah, H.U. Anderson, D.M. Sparlin, S.R. Sehlin, Structure and electrical properties of $La_{1-x}Sr_xCo_{1-y}Fe_yO_3$. Part 2. The system $La_{1-x}Sr_xCo_{0.2}Fe_{0.8}O_3$, Solid State Ionics 76 (1995) 273–283.

[14] J. Yoo, S.-K. Woo, J.H. Yu, S. Lee, G.W. Park, $La_{0.8}Sr_{0.2}MnO_3$ and $(Mn_{1.5}Co_{1.5})O_4$ double layer coated by electrophoretic deposition on Crofer22 APU for SOEC interconnect applications, International Journal of Hydrogen Energy 34 (2009) 1542–1547.

[15] P. Herve, T. Ngamou, N. Bahlawane, Chemical vapor deposition and electric characterization of perovskite oxides $LaMO_3$ (M=Co, Fe, Cr and Mn) thin films, Journal of Solid State Chemistry 182 (2009) 849–854.

[16] R. Todorovska, N. Petrova, D. Todorovsky, S.t. Groudeva-Zotova, Spray-pyrolysis deposition of $LaMnO_3$ and $La_{1-x}Ca_xMnO_3$ thin films, Applied Surface Science 252 (2006) 3441–3448.

[17] R.V. Wandekar, B.N. Wani, S.R. Bharadwaj, Crystal structure, electrical conductivity, thermal expansion and compatibility studies of co-substituted lanthanum strontium manganite system, Solid State Sciences 11 (2009) 240–250.

[18] D. Marrero-López, J.C. Ruiz-Morales, P. Núñez, J.C.C. Abrantes, J.R. Frade, Synthesis and characterization of $La_2Mo_2O_9$ obtained from freeze-dried precursors, Journal of Solid State Chemistry 177 (2004) 2378–2386.

[19] D. Marrero-López, J. Canales-Vázquez, J.C. Ruiz-Morales, A. Rodríguez, J.T.S. Irvine, P. Núñez, Synthesis, sinterability and ionic conductivity of nanocrystalline $La_2Mo_2O_9$ powders, Solid State Ionics 176 (2005) 1807–1816.

[20] L.J. van der Pauw, A method of measuring specific resistivity and hall effect of discs of arbitrary shape, Philips Research Reports 13 (1958) 1–9.

[21] J. Deng, L. Zhang, H. Dai, H. He, C.T. Au, Hydrothermally fabricated single-crystalline strontium-substituted lanthanum manganite microcubes for the catalytic combustion of toluene, Journal of Molecular Catalysis A: Chemical 299 (2009) 60–67.

[22] R.K. Gupta, I.-J. Choi, Y.-S. Cho, H.-L. Lee, S.-H. Hyun, Characterization of perovskite-type cathode, $La_{0.75}Sr_{0.25}Mn_{0.95-x}Co_xNi_{0.05}O_{3+\delta}$ ($0.1 \le x \le 0.3$), for intermediate-temperature solid oxide fuel cells, Journal Of Power Sources 87 (2009) 371–377.

[23] T. Mori, N. Kamegashira, The crystal structure of an oxygen-deficient manganite perovskite $La_xSr_{1-x}MnO_{(5+x)/2}$ $(0 \le x \le 0.5)$, Journal of Alloys and Compounds 408–412 (2006) 1210–1213.

[24] D. Kuscer, M. Hrovat, J. Holc, S. Bernik, D. Kolar, Phases in the $LaMnO_{3\pm\delta}$–$SrMnO_{3-\delta}$–$LaAlO_3$ system, Materials Research Bulletin 35 (2000) 2525–2544.

[25] A. Dutta, J. Mukhopadhyay, R.N. Basu, Combustion synthesis and characterization of LSCF-based materials as cathode of interm ediate temperature solid oxide fuel cells, Journal of the European Ceramic Society 29 (2009) 2003–2011.

[26] H.J. Hwang, M. Awano, Preparation of $LaCoO_3$ catalytic thin film by the sol–gel process and its NO decomposition characteristics, Journal of the European Ceramic Society 21 (2001) 2103–2107.

[27] J. Li, Q. Huang, Z.W. Li, L.P. You, S.Y. Xu, C.K. Ong, Microstructure modification and magnetoresistance enhancement by Ag doping in $La_{2/3}Sr_{1/3}MnO_3$ thin films prepared by dual-beam pulsed laser ablation, Journal of PhysicsCondensed Matter 13 (2001) 3419–3431.

[28] P. Herve, T. Ngamou, N. Bahlawane, Chemical vapor deposition and electric characterization of perovskite oxides $LaMO_3$ (M=Co, Fe, Cr and Mn) thin films, Journal of Solid State Chemistry 182 (2009) 849–854.

[29] Y. Takeda, R. Kanno, M. Noda, Y. Tomida, O. Yamamoto, Cathodic polarization phenomena of perovskite oxide electrodes with stabilized zirconia, Journal of the Electrochemical Society 134 (1987) 2656–2661.